Journal of Fluids and Structures (2001) **15,** 607–616
doi:10.1006/jfls.2000.0369, available online at http://www.idealibrary.com on IDEAL®

THE PHYSICAL MECHANISM OF TRANSITION IN BLUFF BODY WAKES

M. C. Thompson

Department of Mechanical Engineering, Monash University
Clayton, VIC 3800, Australia

T. Leweke

Institut de Recherche sur les Phénomènes Hors Equilibre
49, rue Frédéric Joliot-Curie, B.P. 146, F-13384, Marseille Cedex 13, France

AND

C. H. K. Williamson

Sibley School of Mechanical & Aerospace Engineering, Cornell University
Ithaca, NY 14853-7501, U.S.A.

(Received 24 September 2000, and in final form 28 December 2000)

The physical nature of the initial transition to three-dimensionality of flow past a circular cylinder has been the subject of considerable debate in the literature. Of several proposed mechanisms, the possibility of classification as an elliptical instability is re-examined in this article. Detailed Floquet analysis of the transition shows clear evidence of the growth of an elliptic instability in the forming vortex cores followed by amplification by the strong strain field in the hyperbolic region between the forming and shed vortices. In fact, it appears that the wake immediately behind the cylinder shows distinct signs of a *cooperative elliptic instability* as found previously for interacting counter-rotating vortices. Further downstream, after the vortices have been shed into the wake, the instability again grows in the cores. Three-dimensional simulations provide a semi-quantitative estimate of the "elliptic content" of instability, and confirm that elliptic instability seems to be dominant in the initiation and maintenance of the 3-D perturbation.

1. INTRODUCTION

The two-dimensional wake of a circular cylinder undergoes a hysteretic transition to three-dimensional flow at a Reynolds number $\mathrm{Re} = UD/\nu$ (where U is the free-stream velocity, D the cylinder diameter, and ν the kinematic viscosity) of approximately 190. The initial instability causing this transition gives rise to the first of a sequence of two shedding modes, now generally referred to as modes A and B, which lead to the rapid evolution to fully turbulent flow [see, e.g., Williamson (1996*a*) and Henderson (1997)]. These modes have distinct unstable spanwise wavelength bands and different topologies. There are strong indications that the equivalent of mode A is the initial transition mode for a range of two-dimensional cylindrical bodies, from square cylinders (Robichaux *et al.* 1999) to long plates with aerodynamic noses (Hourigan *et al.* 2001). In addition, modes with the corresponding two distinct spatio-temporal symmetries have been observed in plane wakes both experimentally and numerically (Meiburg & Lasheras 1988). Figure 1 shows visualizations of modes A and B in the cylinder wake, obtained from direct numerical simulations (see Section 3.2).

0889–9746/01/040607 + 10 $35.00/0

Floquet stability analysis indicates that mode A first becomes unstable for a spanwise wavelength of $\lambda = 4D$ at $\mathrm{Re} = 190$ (Barkley & Henderson 1996). This is consistent with experimental flow visualizations of Williamson (1988), which show the spanwise wavelength to be between 3 and 4D. Interestingly, the unstable band of wavelengths becomes broad as the Reynolds number is increased, which may be the underlying cause of dislocations in wakes as observed by Williamson (1992, 1996*a*, *b*). At $\mathrm{Re} = 260$, the Floquet analysis shows that the *two-dimensional* wake becomes unstable to a second shedding mode, mode B (Barkley & Henderson 1996). The critical wavelength in this case is about 0.8D, again consistent with experimental observations of Williamson (1988). In a real flow, this transition occurs at a lower Reynolds number (Williamson 1988), because the development of mode A shedding substantially alters the assumed two-dimensional base flow, so that by $\mathrm{Re} = 230$–240 the wake shows clear evidence of both modes, and of their non-linear interaction. Unlike mode A, mode B appears to remain unstable over a relatively small wavelength band, even at much higher Reynolds numbers. The remnants of mode B can be observed both visually and through spanwise cross-correlation measurements at $\mathrm{Re} = 1000$, when the wake is certainly fully turbulent (Wu *et al.* 1996).

Despite the large number of experimental, theoretical and numerical studies of this 3-D transition, the precise physical nature of the secondary instabilities is not fully understood and has generated much debate. Several possible mechanisms have been proposed. Leweke & Provansal (1995) used a Ginzburg–Landau equation to model the wake as a collection of coupled oscillators. They proposed that the transition was due to a Benjamin–Feir instability found in such systems of oscillators. This was consistent with experiments into the dynamics of the wake; however, this instability has a vanishing spanwise wavenumber inconsistent with the observations of Williamson (1988), and numerical predictions of Barkley & Henderson (1996) of a finite wavenumber. Brede *et al.* (1996) suggested that the strong curvature of the streamlines in the near-wake, and especially of the braid regions between the rollers, was consistent with a centrifugal instability. However, no conclusive evidence was supplied to support this speculation. Karniadakis & Triantafyllou (1992) suggested that the route to turbulence was through period-doubling of the mode B instability. This conclusion was based on numerical computations on a narrow spanwise domain which suppresses mode A, whereas in a real flow its existence alters the evolution, leading to a faster (and different) route to turbulence (Hourigan *et al.* 1995).

Williamson (1996*b*) realized that the two distinct instabilities should be associated with two different length-scales of the two-dimensional wake flow. The two obvious wake length-scales are the core size of the Kármán vortices and the width of the braids between the rollers. He suggested that mode A instability was associated with an *elliptic* instability of the vortex cores, and that mode B instability was associated with an instability of the braid region (which includes the braid shear layer within the near-wake vortex formation region). Leweke & Williamson (1998*b*) showed that elliptic instability theory predicts the approximate spanwise wavelength of the mode A instability and is consistent with both the topology and the waviness of the core vortices. Henderson (1997) was critical of this proposed mechanism for two main reasons. The numerical simulation of the Floquet mode indicated that the instability is complex, showing strong growth both inside and outside the vortex cores, and hence it would not seem reasonable to classify it in terms of a simple instability of an idealized flow. The primary objection, however, was that the mode appears to have the largest amplitude outside the region in which elliptic instability theory indicates it should grow.

In this paper, we present further evidence that the principal physical origin of mode A instability can be attributed to an elliptic instability of the vortex cores.

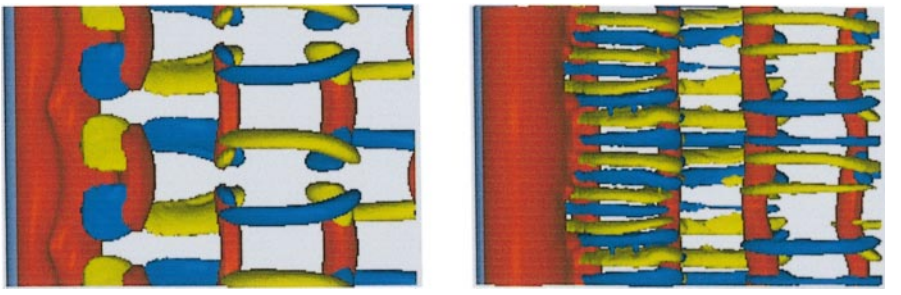

Figure 1. Visualizations of mode A (left, Re = 210) and mode B (right, Re = 250) shedding in the cylinder wake. The green and blue isosurfaces represent positive and negative streamwise vorticity. The flow is from left to right. The front of the circular cylinder is shown at the left of each plot.

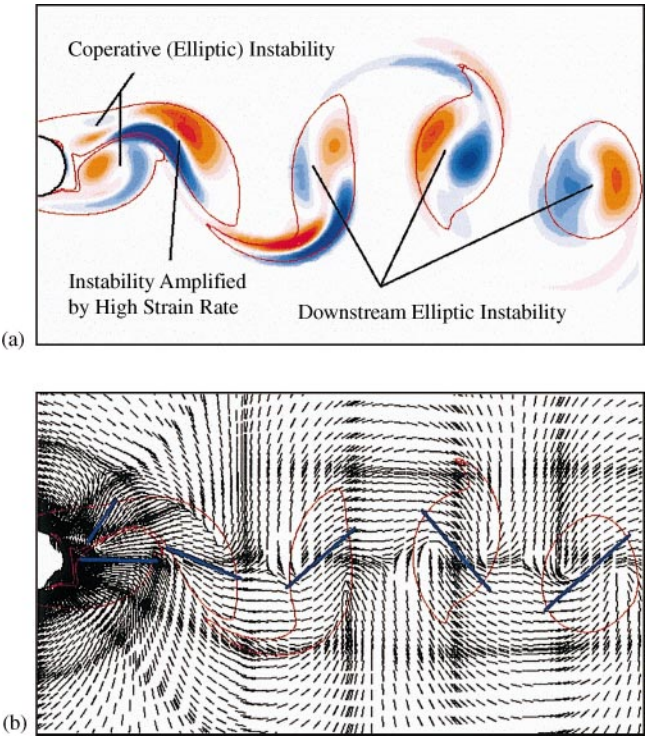

Figure 3. (a) Contour plot of the perturbation spanwise vorticity corresponding to the Floquet mode with spanwise wavelength of $4D$ at Re = 190. (b) Stretching directions of the local strain. The heavy blue lines are indicative of the mean stretching direction through the vortex cores. In both plots, the positions of the wake vortices are indicated by the red lines marking vorticity levels of $\pm 0.2U/D$.

2. REVIEW OF THE ARGUMENTS

The theory of elliptic instability has been developed by Pierrehumbert (1986), Bayly (1986), Landman & Saffman (1987), Waleffe (1990) and others. In its basic form it considers the somewhat idealized case of two-dimensional flow with elliptic streamlines, which are generated by a superposition of a solid-body rotation with constant vorticity ω, and plane strain of magnitude ε. The flow is (i.e., the streamlines are) elliptic if the eccentricity parameter $\beta = 2\varepsilon/|\omega|$ is less than 1, and hyperbolic if $\beta > 1$.

It has been shown by various authors, that such unbounded linear flows are three-dimensionally unstable for all values of β, except $\beta = 1$ (plane Couette flow), which is marginally stable. The mechanism of instability is an amplification of inertial waves in the rotating frame of reference of the base flow through a resonant interaction with the strain field. For inviscid flow, the growth rate σ_i of the most unstable perturbation is given by

$$\frac{\sigma_i}{\varepsilon} = \begin{cases} f(\beta) \approx \frac{9}{16}(1-\beta^m)^n & \text{for } 0 < \beta < 1 \text{ (elliptic flow)}, \\ = \sqrt{1-\beta^{-2}} & \text{for } \beta > 1 \text{ (hyperbolic flow)}. \end{cases} \tag{1}$$

The approximate expression for the elliptic growth rate, with $m = 2{\cdot}811$ and $n = 0{\cdot}3914$, was computed by a least-squares fit of this functional form to the numerical result presented by Landman & Saffman (1987). The expression for the hyperbolic instability are given by Lagnado *et al.* (1984) and Lifshitz & Hamieri (1991). Importantly, although the growth rate depends on the orientation of the three-dimensional perturbation wave vector, it does not depend on its magnitude; i.e., all wavelengths λ are equally unstable. Also note that the growth rate is directly proportional to the magnitude of the strain.

Of course, the wake flow behind a circular cylinder is not an inviscid unbounded linear flow. As shown in Figure 2, the wake consists of finite regions of elliptic flow (primarily the Kármán vortices), and regions of hyperbolic flow (primarily the braid regions between the vortices). It is known, however, from studies by Waleffe (1990) and Leblanc & Godeferd (1998), that there exist localized modes of elliptic and hyperbolic instability that would fit into these regions and effectively "see" a uniform elliptic or hyperbolic flow. The finite core size of the Kármán wake vortices effectively imposes a length scale (the core diameter, which is of the order of D) on the elliptic instability. This, in turn, leads to an effective upper limit on the spanwise wavelength because the length scales in the cross-stream plane and spanwise direction are coupled. [Recent comprehensive accounts on elliptic instability in finite-size vortices in a small strain, i.e. with $\beta \ll 1$, are given by Eloy & Le Dizés (1999, 2001).] In addition, the influence of viscosity imposes a lower limit on the allowable spanwise wavelengths. It was shown in Leweke & Williamson (1998*b*) that the expected spanwise wavelength of an elliptic instability of the Kármán vortices is $\lambda \approx 3D$, given estimates of the average value of β ($\approx 0{\cdot}6$, which is relatively high), and estimates of the

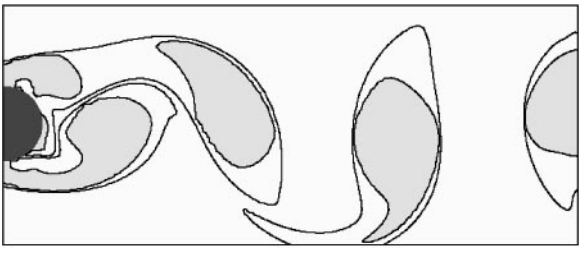

Figure 2. Relation of elliptical flow regions ($\beta < 1$, shown in grey) to the wake vortices (solid lines). The non-elliptic regions are hyperbolic regions (where the strain dominates).

vortex core diameter from direct numerical simulation of the two-dimensional flow. This is respectably in line with the observed experimental determination of $\lambda = 3$–$4D$ and the Floquet analysis of Barkley & Henderson (1996) ($\lambda = 4D$ at onset). The corresponding growth rate can also be evaluated, again using estimates from DNS of the various dependent parameters. In particular, the strain rate was measured to be $\varepsilon D/U \approx 1$ at the center of the near-wake Kármán vortices. The estimated viscous growth rate of elliptic instability in the cylinder wake around $\mathrm{Re} = 200$ is $\sigma D/U \approx 0{\cdot}4$ [see Leweke & Williamson (1998*b*) for more details on these estimates].

Other strong supporting evidence is the apparent existence of invariant stream tubes as indicated by dye visualizations, surrounding the vortex cores, which remain unperturbed despite strong internal waviness of the cores (Leweke & Williamson 1998*b*). This peculiar spatial structure is a characteristic feature of the elliptic instability perturbation.

3. NEW RESULTS AND DISCUSSION

In this section, we shall present and interpret some new evidence on the nature of the initial instability from well-resolved Floquet stability analysis and direct numerical simulations of the transition.

3.1. Floquet Analysis of Mode A Transition

Floquet analysis determines three-dimensional stability of a periodic two-dimensional base flow by solving the linearized Navier–Stokes equations for the perturbation velocity and pressure fields. The present implementation is similar to that described in Barkley & Henderson (1996). The aim is to determine the growth of spanwise sinusoidal perturbations over one shedding period, as a function of Reynolds number and wavelength. The stability is determined by the Floquet multiplier, the multiplication factor connecting the amplitude of a given mode from one cycle to the next. When a multiplier exceeds unity, the corresponding mode becomes unstable. As determined by Barkley & Henderson (1996), the first Floquet multiplier becomes greater than 1 at the transition Reynolds number of 190, with a three-dimensional unstable mode of wavelength $\lambda = 4D$.

Figure 3(a) shows the Floquet instability mode at a certain time in the shedding cycle for $\mathrm{Re} = 190$ and for a Floquet wavelength of $4D$. For these parameters, the corresponding Floquet multiplier was determined to be approximately unity, consistent with the analysis of Barkley & Henderson (1996). It is this instability mode that is responsible for the transition to three-dimensional flow. In effect, the saturated Floquet mode corresponds to mode A.

The plot shows the perturbation spanwise vorticity. Several features of the flow have been marked. Immediately downstream of the cylinder, the wake shows local vorticity distributions reminiscent of the pattern characteristic of elliptic instability. The initial vortex structure in the lower half of the wake, shows the separation of positive and negative perturbation vorticity in the direction of the principal axis of strain [see Figure 3(b)], corresponding to a movement of the centre of the forming roller in the same direction, as is expected for elliptic instability. On the top half of the wake, there is another separation of positive and negative vorticity, again aligned with the strain field. The two localized perturbations together appear to be similar to the cooperative elliptic instability of two interacting counter-rotating vortices (Leweke & Williamson 1998*a*). In particular, they show the same topology and alignment with the local strain field. At this stage of vortex formation, both local perturbations are embedded in elliptic regions of the flow.

Figure 4(a) shows a greyscale plot of the local growth rate of the instability calculated using results from Landman & Saffman (1987). The vorticity and strain distributions are far from the constant values assumed in this study, nevertheless, the distribution is suggestive that the elliptical regions shown in Figure 3(a) are likely to be (elliptically) unstable.

The magnitude of the local strain is given in Figure 4(b). Interestingly, apart from the separating shear layers attached to the cylinder, the strain is large in the hyperbolic region between the two elliptic regions in the top half of the wake at the rear of the cylinder. This is important because the inviscid growth rate roughly scales with the strain rate, so high strain is an indication of high growth rates for both elliptic and hyperbolic instabilities.

Figure 5 shows a sequence of the images of the development of the spanwise vorticity perturbation close to the back of the cylinder. Initially, the perturbations develop in each elliptic region resulting in the generation of positive and negative perturbation vorticity on each side of the core centre. This is indicative of the movement of the core in the direction of principal strain as occurs for elliptical instability. For both the finite-size vortex examined by Waleffe (1990), and the cooperative elliptic instability studied by Leweke & Williamson (1998*a*), the perturbation growth (at least for a reasonable time) is limited to the elliptical regions of the flow. This is not true in this case. Here, although the initial development of the instability occurs in the forming vortex cores, the individual perturbations merge and grow strongly between the elliptical regions. This is not surprising as the region between the forming vortex structures, and especially towards the downstream limits of the structures, is strongly strained as can be seen from Figure 4(b). It appears that this high strain rate leads to strong amplification of the perturbation. As the merged perturbation is advected downstream, it appears to lag behind the advected vortex cores. This is probably due to a combination of two factors: (i) the mean wake velocity defect of the perturbation on the side of the cores closer to the wake centre line is advected downstream less quickly than the more off-centred parts or the cores themselves; (ii) the instability is preferentially amplified in the highly strained hyperbolic region *between* vortex structures from the same side of the wake. The end result is that, after the vortex has been shed into the wake, the maximum amplitude of the instability is in the braid regions rather than the vortex cores. This maximal amplitude occurring between the forming vortices and in the braid regions was noticed by Henderson (1997), and helped lead to the conclusion that the instability should not be classified as elliptic. It needs to be pointed out that unless resolution is adequate and the contour levels are chosen carefully, the initial development of the instability in the core regions can easily be overlooked.

As the vortices move further downstream, out of the formation region, they maintain their alignment and shape to a large extent and so are ideal candidates for a second elliptic instability. Initially, they are relatively perturbation-free, but the background perturbation

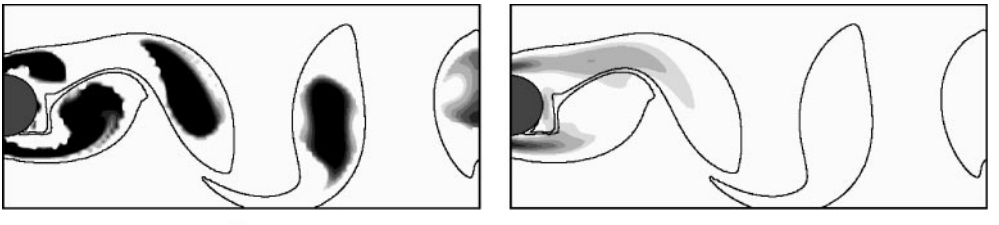

Figure 4. Contour plots of (a) the viscous growth rate predicted from elliptic instability theory (Landman & Saffman 1987), and (b) the strain magnitude showing that the strain maintains a high value in the hyperbolic region (between the two elliptic regions in the top half of the wake, immediately behind the cylinder).

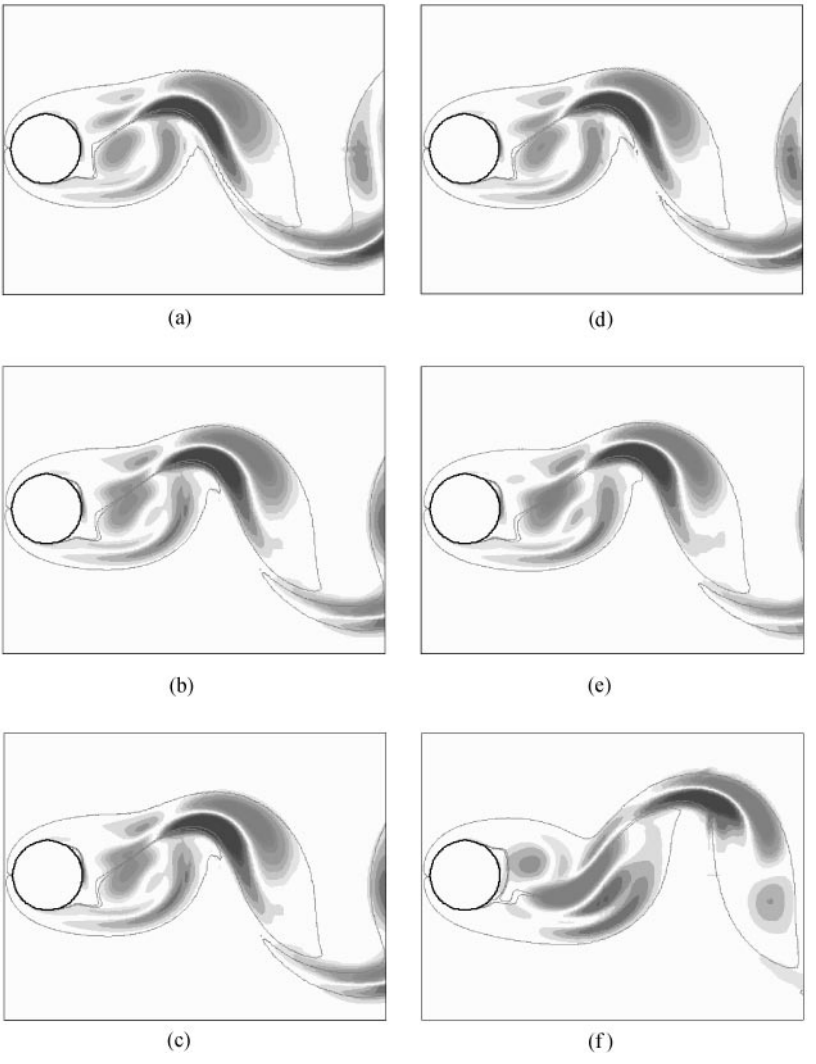

Figure 5. Development of the instability during the shedding process. Relative to the first (a), the subsequent images (b–f) are 0.04, 0.08, 0.12, 0.24 and 0.32 shedding periods later, respectively.

field leads to the rapid development of elliptic instability in the cores. Although the cores, by no means, have constant local vorticity and strain fields, they clearly show a perturbation field consistent with the vorticity distribution expected from elliptic instability. This rapid growth only occurs for a short time. Approximately one period further downstream, viscous growth rate calculations indicate that the instability is only marginally unstable. This is consistent with the observed development shown in Figure 3(b) (and further downstream).

It is possible to estimate the growth rates for the initial cooperative and the downstream elliptic instabilities from the simulations. This was done by measuring the rate of change of the circulation in each half of the bipolar spanwise perturbation vorticity of the cores over approximately one quarter of a shedding cycle. The line integral defining this circulation was evaluated numerically for at least five consecutive snapshots in time spaced 0·05 cycles apart. For the initial cooperative core instability, and downstream elliptic core instability, the growth rate was calculated to be $\sigma D/U = 0{\cdot}39$ and 0·42, respectively. Although there is

some uncertainty in these estimates, they are in good agreement with the theoretical estimate $\sigma D/U \approx 0{\cdot}4$ given above.

In summary, an interpretation of the evidence is that there are two elliptic instabilities, contributing to the mode A transition. The first occurs immediately at the back of the cylinder as the Kármán vortices are forming, and the second further downstream as the vortices are shed into the wake. Although the first instability does not persist in the elliptic region, and appears to be amplified in the hyperbolic region, it seems likely that the spanwise wavelength is selected according to the scale of the Kármán vortices in line with elliptic instability theory. Both when the perturbation is initially forming in the core regions, and when it is undergoing amplification in the hyperbolic region, it appears that the growth is due to the action of the strain field. This is consistent with the physical mechanism responsible for both elliptic and hyperbolic instability.

3.2. Three-Dimensional Direct Numerical Simulation

As further support for the importance of the elliptical nature of the instability, direct numerical simulations were performed. The same three-dimensional spectral/spectral-element code used for previous wake transition simulations (Thompson *et al.* 1996) is used here. Spectral elements are used in the cross-stream planes and a Galerkin Fourier expansion in the spanwise direction. Care was taken to ensure adequate resolution and domain size to capture the essential physics of the mode A transition. However, due to space limitations, these validation studies are not described here. The spanwise domain size was chosen to be $4D$ to approximately match the most unstable wavelength of the spanwise mode at transition. This limits the possible wavelengths represented by the Fourier expansion to be $4D/n$ ($n = 1, 2, \ldots$). Of these wavelengths only $\lambda = 4D$ is unstable at the Reynolds number of the simulations.

A three-dimensional simulation of mode A at $\mathrm{Re} = 200$ was started by extending the flow field from a previous two-dimensional simulation to the three-dimensional domain. To initiate the development of three-dimensionality, the field was perturbed by adding random noise at a relative level of 10^{-4} to the velocity field. The flow was then evolved for sufficient time (approximately 10 shedding cycles), so that it effectively consisted of the two-dimensional base flow plus the most unstable Floquet mode. At this stage, the relative amplitude of perturbation field is still very small and the evolving flow is well within the linear regime where the growth is governed by the Floquet multiplier.

At this point in the temporal development of the mode A flow, the perturbation field was decomposed into two mutually exclusive components. The first perturbation field is only nonzero where the two-dimensional flow (shown in Figure 2) is elliptic ($\beta < 1$), and the second where it is hyperbolic ($\beta > 1$). From these two perturbation fields, two three-dimensional flow fields were constructed by adding the spanwise-averaged (two-dimensional) base flow to the *elliptic* and *hyperbolic* perturbation fields, respectively. Thus, the first flow field contains the elliptic part of the perturbation, while the second contains the hyperbolic part. This split-up was performed at a random time in the shedding cycle. The results that follow may, to a certain degree, depend on the choice of this time, a point which was not investigated further so far. (Formally, regions with $\beta < 1$ may also develop instabilities linked to centrifugal effects. However, no attempt was made here to further isolate these effects from those of the elliptic instability.)

Using the two fields as initial conditions, the flow was evolved for several more shedding cycles. Figure 6(a,b) show isosurface visualizations of the perturbation spanwise vorticity after 2·4 shedding cycles, for the two initial fields. The isosurface level is the same in both cases. These visualizations show that the vorticity field that has evolved from the initially

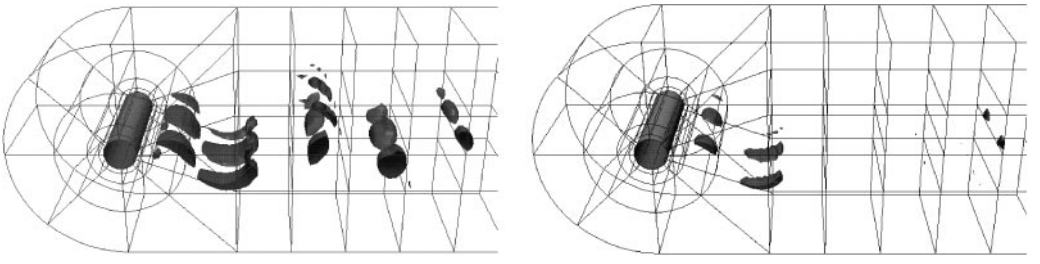

Figure 6. Isosurface visualization of the perturbation spanwise vorticity after removing (a) the hyperbolic or (b) the elliptic component of the Floquet mode and evolving the flow for 2.4 shedding periods.

elliptic field recovers towards the complete Floquet mode much more quickly than the initially hyperbolic one. In particular, starting from the "elliptic" conditions, the perturbation in the hyperbolic braids, initially set to zero, reappears very rapidly. On the contrary, with the "hyperbolic" initial field, i.e., in the absence of the elliptic core deformations, the perturbations in the braids actually *decrease* in the first few cycles of the simulation. Thus, it appears that the elliptic instability of the vortex cores in the wake formation zone has a dominant influence on the development of the instability.

The "degree of ellipticity" can be approximately quantified through the following argument. Let $\Phi_0, \Phi_1, \Phi_2, \ldots$ be the Floquet modes of the linearized Navier–Stokes equations, where the modes have been ordered according to magnitude of the eigenvalues (the Floquet multipliers) from largest to smallest. In particular, Φ_0 corresponds to the only growing mode, i.e., the one responsible for the mode A transition. To form the two initial fields, this Floquet mode is split into two mutually exclusive components Φ_e (elliptic) and Φ_h (hyperbolic): $\Phi_0 = \Phi_e + \Phi_h$. We can now expand these two components in terms of all the Floquet modes:

$$\Phi_e = \sum \alpha_i \Phi_i \quad \text{and} \quad \Phi_h = \sum \gamma_i \Phi_i. \tag{2}$$

From the definition of Φ_e and Φ_h the following relationships exist between the expansion coefficients: $\alpha_0 + \gamma_0 = 1$ and $\alpha_i + \gamma_i = 0$, for $i > 0$. Effectively, α_0/γ_0 determines the ratio of elliptic to hyperbolic "contents" of the growing Floquet mode. After each shedding period, the amplitude of each Floquet mode is multiplied by its Floquet multiplier, i.e., after many shedding cycles the perturbation evolves towards Φ_0, the multipliers of the other modes being less than 1. Thus, the ratio α_0/γ_0 is given by the ratio of the amplitudes of the two growing perturbations starting from the elliptic and hyperbolic conditions described above, after the same number of periods. In the present simulations, this ratio was measured eight shedding cycles after initialization, which is sufficient to damp out the contribution from the stable Floquet modes (Φ_i, $i > 0$), whose multipliers are all smaller than 0·2 at $\mathrm{Re} = 200$ (Barkley & Henderson 1996). The result is $\alpha_0/\gamma_0 = 2{\cdot}03$. In this sense, the Floquet mode responsible for mode A transition may be characterized as being about two-thirds elliptic and one-third hyperbolic.

4. CONCLUSIONS

It is useful, where possible, to attribute a flow transition to a simple physical mechanism applicable to idealized flows, because it aids with providing a physical understanding of the transition. This is valuable for interpreting other related (or unrelated) transitions. It is with this aim that we have attempted to interpret the transition to three-dimensionality for flow

past a circular cylinder. Importantly, there is now considerable evidence that the same transition scenario applies to a whole range of two-dimensional body geometries. Certainly, the transition is complex, the instability is not restricted to the forming vortices and the Kármán vortices in the wake, and even within the cores the ellipticity parameter is far from constant. In addition, linear stability analysis predicts that the unstable mode grows as a whole, rather than as a set of effectively decoupled regions with their own local physical instabilities triggering instabilities in other regions. Nevertheless, the evidence presented in this paper shows that the first instability to form as the fluid advects downstream past the cylinder occurs in the forming vortex cores, with a growth rate and spanwise wavelength close to those predicted by idealized elliptic instability theory. This initial instability shows distinct features similar to the cooperative elliptic instability found by Leweke & Williamson (1998*a*) for two counter-rotating vortices. Because of the complexity of the flow, it appears that the nascent perturbation is amplified in the highly strained hyperbolic region between forming vortices, leading to the observed high perturbation amplitudes in the braids. A second elliptic instability develops in the cores of the fully formed Kármán vortices further downstream. Direct numerical simulations, carried out to analyse the contributions of elliptic and hyperbolic flow regions to the three-dimensional transition, support the interpretation that the elliptic instability is dominant in the initiation and maintenance of the mode A perturbation.

References

Barkley, D. & Henderson, R. D. 1996 Three-dimensional Floquet stability analysis of the wake of a circular cylinder. *Journal of Fluid Mechanics* **322,** 215–241.

Bayly, B. J. 1986 Three-dimensional instability of elliptical flow. *Physical Review Letters* **57,** 2160–2163.

Brede, M., Eckelmann, H. & Rockwell, D. 1996 On secondary vortices in a cylinder wake. *Physics of Fluids* **8,** 2117–2124.

Eloy, C. & Le Dizès, 1999 Three-dimensional instability of Burgers and Lamb–Oseen vortices in a strain field. *Journal of Fluid Mechanics* **378,** 145–166.

Eloy, C. & Le Dizès, 2001 Stability of the Rankine vortex in a multipolar strain field. *Physics of Fluids* **13,** 660–676.

Henderson, R. D. 1997 Nonlinear dynamics and pattern formation in turbulent wake transition. *Journal of Fluid Mechanics* **352,** 65–112.

Hourigan, K., Thompson, M. C. & Sheridan, J. 1995 The development of three-dimensionality in the wake of a circular cylinder. In *Advances in Turbulence V* (ed. R. Benzi), pp. 496–501. Dordrecht: Kluwer Academic.

Hourigan, K., Thompson, M. C. & Tan, B. T. 2001 Self-sustained oscillations in flows around long blunt plates. *Journal of Fluids and Structures* **15,** xxx–xxx (this issue).

Karniadakis, G. E. & Triantafyllou, G. S. 1992 Three-dimensional dynamics and transition to turbulence in the wake of bluff objects. *Journal of Fluid Mechanics* **238,** 1–30.

Lagnado, R. R., Phan-Thien, N. & Leal, L. G. 1984 The stability of two-dimensional linear flows. *Physics of Fluids*, **27,** 1094–1101.

Landman, M. J. & Saffman, P. G. 1987 The three-dimensional instability of strained vortices in a viscous fluid. *Physics of Fluids* **30,** 2339–2342.

Leblanc, S. & Godeferd, F. S. 1988 An illustration of the link between ribs and hyperbolic instability. *Physics of Fluids* **11,** 497–499.

Leweke, T. & Provansal, M. 1995 The flow behind rings: bluff body wakes without end effects. *Journal of Fluid Mechanics* **288,** 265–310.

Leweke, T. & Williamson, C. H. K. 1998*a* Cooperative elliptic instability of a vortex pair. *Journal of Fluid Mechanics* **360,** 85–119.

Leweke, T. & Williamson, C. H. K. 1998*b* Three-dimensional instabilities in wake transition. *European Journal of Mechanics B/Fluids* **17,** 571–586.

Lifschitz, A. & Hameiri, E. 1991 Local stability conditions in fluid dynamics. *Physics of Fluids* A **3,** 2644–2651.

MEIBURG, E. & LASHERAS, J. C. 1988. Experimental and numerical investigation of the three-dimensional transition in plane wakes. *Journal of Fluid Mechanics* **190,** 1–37.

PIERREHUMBERT, R. T. 1986 Universal short-wave instability of two-dimensional eddies in an inviscid fluid. *Physical Review Letters* **57,** 2157–2159.

ROBICHAUX, J., BALACHANDAR, S. & VANKA, S. P. 1999 Three-dimensional Floquet instability of the wake of a square cylinder. *Physics of Fluids* **11,** 560–578.

THOMPSON, M. C., HOURIGAN, K. & SHERIDAN, J. 1996 Three-dimensional instabilities in the wake of a circular cylinder. *Experimental Thermal and Fluid Science* **12,** 190–196.

WALEFFE, F. 1990 On the three-dimensional instability of strained vortices. *Physics of Fluids* A **2,** 76–80.

WILLIAMSON, C. H. K. 1988 The existence of two stages in the transition to three-dimensionality of a cylinder wake. *Physics of Fluids* **31,** 3165–3168.

WILLIAMSON, C. H. K. 1992 The natural and forced formation of spot-like vortex dislocations in the transition of a wake. *Journal of Fluid Mechanics* **243,** 393–441.

WILLIAMSON, C. H. K. 1996*a* Vortex dynamics in the cylinder wake. *Annual Review of Fluid Mechanics* **28,** 477–526.

WILLIAMSON, C. H. K. 1996*b* Three-dimensional wake transition. *Journal of Fluid Mechanics* **328,** 345–407.

WU, J., SHERIDAN, J., WELSH, M. C. & HOURIGAN, 1996 Three-dimensional vortex structures in a cylinder wake. *Journal of Fluid Mechanics* **312,** 201–222.